Journal of Sound and Vibration (1998) **218**(3), 419–444
Article No. sv981861

DISCRETE HUYGENS' MODEL APPROACH TO SOUND WAVE PROPAGATION

Y. KAGAWA, T. TSUCHIYA, B. FUJII† AND K. FUJIOKA‡

Department of Electrical and Electronic Engineering, *Okayama University*,
3-1-1 *Tsushima-naka*, *Okayama* 700, *Japan*

(*Received* 14 *January* 1998, *and in final form* 16 *June* 1998)

A transmission-line matrix (TLM) model is applied to the simulation of sound wave propagation. Two-dimensional and axisymmetric TLM elements are first developed for both linear and non-linear sound field applications. A digital filter expression equivalent to the two-dimensional TLM element is also developed. The program is implemented on a computer and the validity and accuracy of the model are examined for a plane wave in an acoustic tube. Some simulated examples are then demonstrated for the two-dimensional and axisymmetric sound wave propagation problems. The results are compared with finite element solutions. To cope with the ambiguity of discretization errors, the introduction of Gaussian filtering capability is proposed.

1. INTRODUCTION

Sound wave propagation and radiation problems lead to the solution of the wave equation in the time domain or Helmholtz equation in the frequency domain under the proper boundary conditions. As analytical solutions are not always possible for general boundary shape and conditions, the numerical approach must be adopted by the use of finite difference, finite element or boundary element method. They can be said to be based on the mathematical or numerical modelling in which the differential equation is numerically solved.

On the other hand, there is the alternative simulation approach based on physical modelling in which the process of a phenomenon is honestly traced. The discrete Huygens' model is a good candidate for this approach. According to Huygens, a wave front consists of a number of secondary radiators which give rise to spherical wavelets. The envelope of these wavelets forms a new spherical wave front. As a consequence of the repetiton of this mechanism, Huygens explained the cause of the wave propagation. This process can be directly implemented on a digital computer for a field discretized in time and space. The discrete Huygens' model is a synonym for the Transmission-Line Matrix method or Transmission-

† Present address: Nikon Corporation, Tokyo, Japan.
‡ Present address: Nippon Telegraph and Telephone Corporation, Chugoku-branch, Hiroshima, Japan.

0022–460X/98/480419 + 26 $30.00/0

Line Matrix model (TLM). The method is inherently a time domain approach, which does not require the solution of the differential equation.

The TLM method was first developed by P. B. Johns applied to electromagnetic waveguide problems [1, 2]. The name is given after the equivalence between the electromagnetic field equations and the transmission line circuit equations. The development has been well documented in the literature by Hoefer [3, 4], Sadiku and Agba [5] and others [6]. One of the present authors had tried the application of the method to the acoustic field problems but without much success due to the immature capability of the computer [7, 8]. Saleh and Blanchfield [9] recently applied the method to the acoustic radiation from array transducers. The circuit theory and electromagnetic field theory have historically been developed independently and have also been taught separately, but the circuits are essentially the spatially discrete expression of continuum fields. The acoustical engineers sometimes preferred the equivalent circuit approach to the analysis and the design of electro-acoustic devices. The finite element equivalent circuit expression to the acoustic fields have been reported [10, 11].

The present paper discusses the application of the transmission-line matrix method or a Huygens' discrete model to the acoustic field problems. The fundamental characteristic of the sound wave in the transmission-line modelling is examined, and then the analysis is extended to include the non-linear effect due to the pressure for the intense sound wave field with some examples.

2. THEORY

2.1. DISCRETE HUYGENS' MODEL AND TLM MODEL [3, 4]

We consider here the sound wave propagation radiated from a point source as shown in Figure 1, in which the sound wave radiates spherically from the point source. According to Huygens, a wave front consists of a number of secondary point sources which give rise to spherical wavelets, and the envelope of these wavelets forms a new spherical wavefront which again gives rise to a new generation of spherical wavelets.

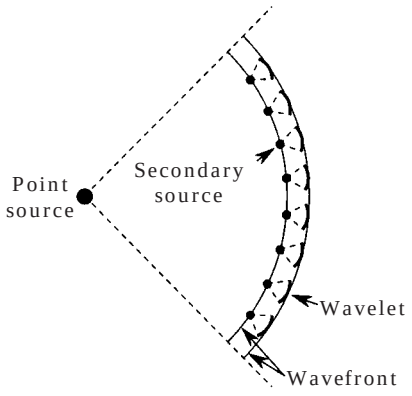

Figure 1. Huygens' principle.

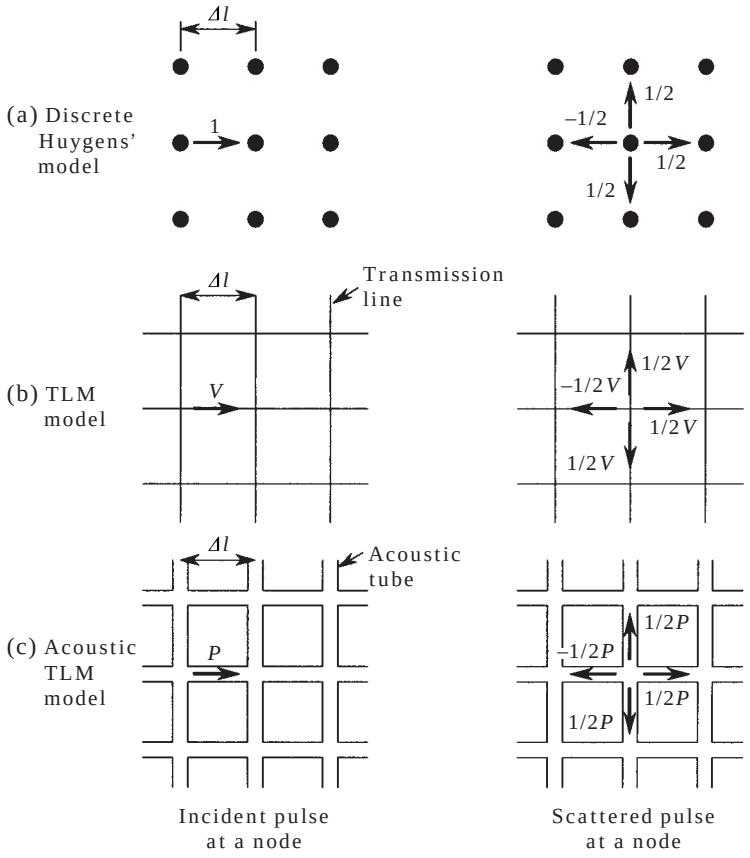

Figure 2. Discrete Huygens' model and TLM models.

Now we consider the Huygens' principle in the discrete sense in order to implement this process of sequences on a digital computer. The two-dimensional sound space is first considered in which the above mentioned process occurs adhering to the Cartesian coordinates directions. An array of nodes and mesh which are separated by the distance Δl are shown in the left figure of Figure 2(a). The propagation takes place between isolated nodes of the matrix. When a sound-impulse of unit amplitude or delta function is incident on one of the nodes, the sound-impulses scatter in four directions as shown in the right figure of Figure 2(a) like a collision of elastic balls. Each scattered pulse has one-quarter of the incident energy, and thus the magnitude of the scattered pulse is 1/2, in which the coefficient of the reflected one to the incident direction is negative.

This is equivalent to the travelling of the pulses over an orthogonal mesh made of pairs of transmission lines, or TLM as shown in Figure 2(b). A pair of orthogonally connected transmission lines forms impedance discontinuity at the node because the characteristic impedance is the same for each branch and three branches are connected in parallel to one at the node, so that the impedance from one node is one-third of that of the incidence branch. When a voltage-impulse of amplitude V is incident on one of the branches, the scattering similar to what is

shown in Figure 2(a) takes place at the node due to impedance discontinuity. Acoustical analogy is depicted in Figure 2(c), as the transmission lines correspond to the thin acoustic tubes. The crossed acoustic tubes also form impedance discontinuity at their junction, so that the same sort of scattering also takes place.

We then proceed to the more general case in which four impulses $P^1 \sim P^4$ are incident to the four branches at the same time $t = k\Delta t$ (where $\Delta t = \Delta l/c$ is the time delay required for a pulse to travel the distance Δl, c is propagation speed along the branch and k is the integer) as shown in Figure 3(a). The response can be obtained by superposing the contribution from all branches. The scattered impulse S^n at branch n at time $t + \Delta t = (k + 1)\Delta t$ is given as

$$ {}_{k+1}S^n = \frac{1}{2}\sum_{m=1}^{4} {}_kP^m - {}_kP^n \tag{1} $$

where ${}_kP^n$ is incident impulse at the branch n at time $t = k\Delta t$. This equation can be rewritten in the expression of a scattering matrix as

$$ {}_{k+1}\begin{bmatrix} S^1 \\ S^2 \\ S^3 \\ S^4 \end{bmatrix} = \frac{1}{2}\begin{bmatrix} -1 & 1 & 1 & 1 \\ 1 & -1 & 1 & 1 \\ 1 & 1 & -1 & 1 \\ 1 & 1 & 1 & -1 \end{bmatrix} {}_k\begin{bmatrix} P^1 \\ P^2 \\ P^3 \\ P^4 \end{bmatrix}. \tag{2} $$

Pressure $P_{i,j}$ at the node is given by

$$ {}_kP_{i,j} = \frac{1}{2}\sum_{n=1}^{4} {}_kP^n \tag{3} $$

where subscripts i, j represent the node position $(x, y) = (i\Delta l, j\Delta l)$.

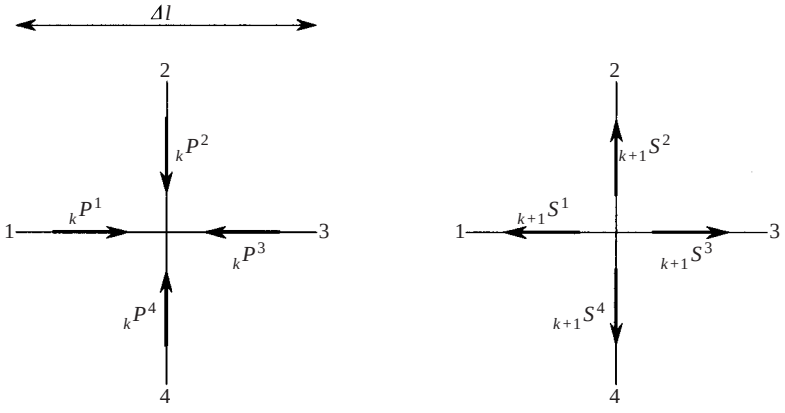

(a) Incidence at time k (b) Scattering at time $k+1$

Figure 3. Scattering at a node.

The scattered pulses travel along the branches in the reversal directions. When the field is divided into square meshes, the scattered pulses become incident pulses to the adjacent elements at whose node scattering again takes place. The incident pulses on a node at position (i, j) are represented by the scattered pulses at the adjacent nodes as

$$
\begin{aligned}
{}_{k+1}P^1_{i,j} &= {}_{k+1}S^3_{i-1,j}, \quad {}_{k+1}P^3_{i,j} = {}_{k+1}S^1_{i+1,j} \\
{}_{k+1}P^2_{i,j} &= {}_{k+1}S^4_{i,j+1}, \quad {}_{k+1}P^4_{i,j} = {}_{k+1}S^2_{i,j-1}.
\end{aligned} \tag{4}
$$

Repeating the operation of equations (2)–(4) on all nodes, the impulse response of the field can be traced at successive time intervals. The method is inherently a time domain solution method which is quite suitable for the simulation and visualization of a wave behavior on the computer. Equation (3) indicates the average theorem given in the finite difference solution of Poisson's equation. The method is numerically equivalent to the FD–TD method. However, TLM provides a physical model, which does not require the solution of the wave equation.

2.2. EQUIVALENT CIRCUIT EXPRESSION OF A TWO-DIMENSIONAL TLM MODELLING

In this section, we intend to find analogue and digital equivalent circuits to the two-dimensional discrete Huygens' model or TLM model.

2.2.1. *Analogous equivalent circuit*

Figure 4 shows the distributed and lumped circuits equivalent to an element of a two-dimesional TLM model. Referring to Figure 4, one applies Kirchhoff's current and voltage laws to derive the line equations in which as $\Delta l \to 0$ we arrive at the following differential equations:

$$
-\frac{\partial I_x}{\partial x} - \frac{\partial I_y}{\partial y} = 2C\frac{\partial V}{\partial t} \tag{5}
$$

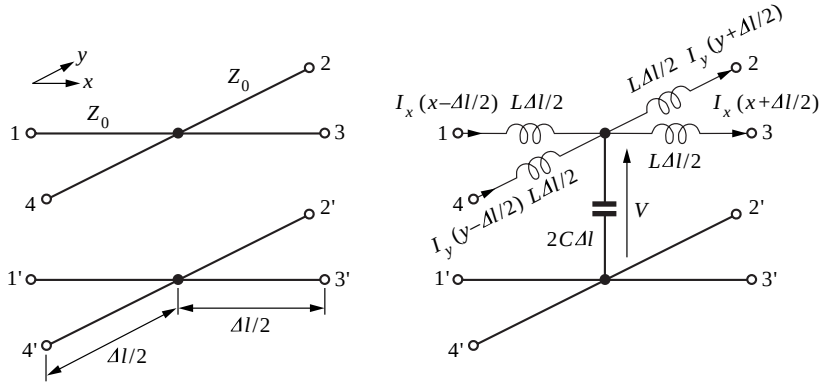

(a) TLM element (b) Equivalent lumped-element model

Figure 4. Two-dimensional TLM element and its equivalent circuit.

$$-\frac{\partial V}{\partial x} = L\frac{\partial I_x}{\partial t}, \quad -\frac{\partial V}{\partial y} = L\frac{\partial I_y}{\partial t} \tag{6}$$

where the line parameters L and C are inductance and capacitance per unit length respectively. These equations are combined to give

$$\frac{\partial^2 V}{\partial x^2} + \frac{\partial^2 V}{\partial y^2} = \frac{1}{c_T^2}\frac{\partial^2 V}{\partial t^2} \tag{7}$$

where $c_T(=1/\sqrt{2LC})$ is propagation speed over the circuit. This is a wave equation in two-dimensional TLM network.

Consideration is then made for the continuity equation and the linear force equation for the two-dimensional sound field, which are

$$-\frac{\partial u_x}{\partial x} - \frac{\partial u_y}{\partial y} = \frac{1}{\kappa}\frac{\partial p}{\partial t} \tag{8}$$

$$-\frac{\partial p}{\partial x} = \rho\frac{\partial u_x}{\partial t}, \quad -\frac{\partial p}{\partial y} = \rho\frac{\partial u_y}{\partial t} \tag{9}$$

where u_x and u_y are the particle velocities in x and y directions, p is the sound pressure, ρ is the mass density and κ is the compressibility. Combining equations (8) and (9), one derives the wave equation with respect to sound pressure p as

$$\frac{\partial^2 p}{\partial x^2} + \frac{\partial^2 p}{\partial y^2} = \frac{1}{c_0^2}\frac{\partial^2 p}{\partial t^2} \tag{10}$$

where $c_0 = \sqrt{\rho/\kappa}$ is the sound speed in free space. Comparing equations (8)–(10) with equations (5)–(7) yields the equivalence between the parameters, which are shown in Table 1. In the above comparison, correspondence exists for ρ and κ to L and $1/2C$ respectively. Therefore, the correspondence for the propagation speed is

$$c_T = \frac{1}{\sqrt{2}}c_0. \tag{11}$$

The sound speed of the TLM network is $1/\sqrt{2}$ of the sound speed c_0 in the free space.

To derive the transmission characteristic of the TLM model in frequency domain, a two port network corresponding for a single element on x–z plane is

TABLE 1

Equivalence between acoustic field parameters and transmission line model parameters

Acoustic field parameters	p	u_x	u_y	ρ	$1/\kappa$
Transmission line model parameters	V	I_x	I_y	L	$2C$

used [1]. The voltage V_1 and current I_1 at branch 1 relate to those at branch 3 by the transfer matrix equation given as

$$\begin{bmatrix} V_1 \\ I_1 \end{bmatrix} = \begin{bmatrix} 1 - 4\sin^2(\theta/2) & j2\sin(\theta/2)\cos(\theta/2)\{1 - \tan^2(\theta/2)\}Z_0 \\ j4\sin(\theta/2)\cos(\theta/2)/Z_0 & 1 - 4\sin^2(\theta/2) \end{bmatrix} \begin{bmatrix} V_3 \\ I_3 \end{bmatrix} \tag{12}$$

where $\theta = 2\pi\Delta l/\lambda$ (λ is wavelength), and Z_0 is the characteristic impedance of a branch. If the wave propagates over the periodic structure like TLM network, the propagation constant $\gamma_p = \alpha_p + j\beta_p$ (where α_p is attenuation constant, β_p is phase constant) is given by

$$\cosh(\gamma_p \Delta l) = 1 - 4\sin^2(\theta/2). \tag{13}$$

For the element smaller than the wavelength ($\Delta l/\lambda < 1/4$), the propagation velocity c_p over the two-dimensional TLM network is given as

$$c_p = c_0 \frac{\pi\Delta l}{\lambda \sin^{-1}\left\{\sqrt{2}\sin\left(\dfrac{\pi\Delta l}{\lambda}\right)\right\}} \tag{14}$$

The propagation velocity has dispersion characteristics. For the very low frequency range ($\Delta l/\lambda \ll 1/4$), the propagation velocity in the two-dimensional network approaches $c_0/\sqrt{2}$, which agrees with equation (11), while the propagation speed becomes lower as it goes into the higher frequency. The cutoff frequency is $\Delta l/\lambda = 0{\cdot}25$.

2.2.2. *Digital equivalent circuit*

In the TLM model, the sound propagation is simulated as the consequence of the impulses in each element. In this section a multi-port digital filter modelling whose impulse response is equivalent to equation (2) is proposed.

The digital filter equivalence is shown in Figure 5. This is the FIR digital filter. As in the previous section, consideration is also given to sound propagation in a plane wave or one-dimensional field. To consider the one-dimensional case, input and output ports are taken at port 1 and 3 which are open-circuited while the branches 2 and 4 are short-circuited, which corresponds to the boundary condition on a rigid wall. Under these circumstances, P^1 is applied to port 1, and the impulse response at port 3 at time $t = k\Delta t$ is given from equation (2) as

$${}_kS^3 = \tfrac{1}{2}({}_{k-1}P^1 + {}_{k-2}P^1). \tag{15}$$

Applying the z transformation to this expression, the transfer function is given as

$$\tilde{H}(z) = \tfrac{1}{2}z^{-1}(1 + z^{-1}) \tag{16}$$

Substituting $z = e^{j2\pi(\Delta l/\lambda)}$, one derives the following transfer frequency characteristic

$$\tilde{H}(e^{j2\pi(\Delta l/\lambda)}) = \cos\left(\pi\frac{\Delta l}{\lambda}\right) e^{j3\pi(\Delta l/\lambda)}. \tag{17}$$

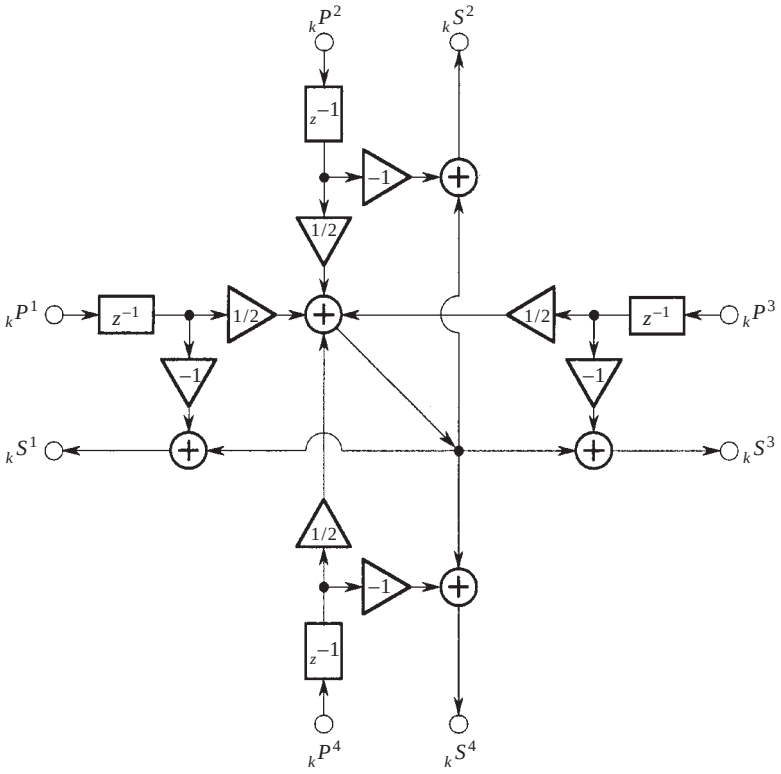

Figure 5. Digital circuit equivalent to a TLM element.

The characteristics is shown in Figure 6 (bold lines). In the figure, the phase characteristic corresponds to the propagation speed normalized by the speed c_0 in free space. The amplitude characteristic is of the low-pass filter. The propagation speed is almost independent of the frequency with the value of $0{\cdot}667c_0$. This is slightly smaller than $c_0/\sqrt{2}$ of the analogous equivalent circuit. The characteristics

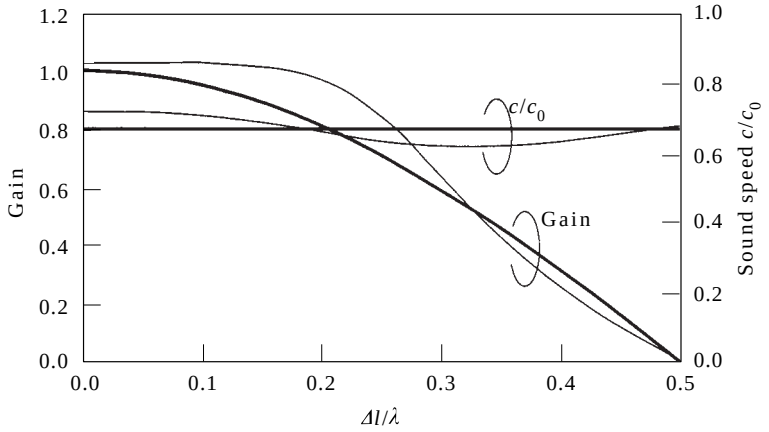

Figure 6. Transfer characteristics of the digital filter equivalent to the TLM model for plane wave or one-dimensional sound propagation field. ——, open circuit, ——, reflectionless termination.

evaluated by the Fourier transformation of the impulse response of the TLM element is in agreement with what is shown in Figure 6. The digital filter model is thus appropriate for the equivalent expression of the TLM model.

The sound propagation in the one-dimensional field of infinite length or without reflection is then considered. To provide the reflectionless boundary, ports 1 and 3 must be terminated by the characteristic impedance which is created by a certain feedback loop to provide the scattering from the adjacent nodes. The transfer function in z-domain is given by

$$\tilde{H}(z) = \frac{1}{2}\frac{z^{-1}(1+z^{-1})}{(1+az^{-1})(1-az^{-2})} \tag{18}$$

where a is the gain of the feedback loop. For the non-reflective termination, the parameter a is chosen to be $(1-\sqrt{2})/(1+\sqrt{2})$. The transfer frequency characteristic is evaluated by

$$\tilde{H}(e^{j2\pi(\Delta l/\lambda)}) = \cos\left(\pi\frac{\Delta l}{\lambda}\right)\frac{e^{j3\pi(\Delta l/\lambda)}}{(1+ae^{j2\pi(\Delta l/\lambda)})(1-ae^{j4\pi(\Delta l/\lambda)})}. \tag{19}$$

The frequency characteristics calculated by equation (19) is shown in Figure 6 (fine lines), which again shows a low pass filter characteristic. The amplitude is flat in the lower pass band ($\Delta l/\lambda < 0{\cdot}2$) whose value is about 3% larger than a unit. The error occurs due to the fact that the boundary is not perfectly reflectionless. The propagation speed now slightly depends on the frequency. The speed in the lower frequency range is however in good agreement with that of the analogous equivalent circuit ($c_0/\sqrt{2}$).

2.3. MODELLING OF THE BOUNDARIES

In the previous chapter, we introduced some boundary conditions without explicit explanation. We next discuss the boundary conditions. The boundaries to be considered here are the cases of a rigid wall, a sound absorbing wall and a wall driven by the velocity source. In TLM modelling, these boundaries are usually placed halfway between two nodes or at the ends of the element's branch arms as shown in Figure 7 which can be achieved there by introducing the reflection coefficient R.

For the rigid wall, the reflection coefficient R is 1, so that the end of branch n which faces the rigid wall must be open circuited as shown in Figure 7(a). To implement this condition, the following relation is applied:

$$_kP^n = {}_kS^n. \tag{20}$$

For the sound absorbing wall, the boundary is terminated with a resistive load Z_a. The reflection coefficient is defined as

$$R = \frac{Z_a - Z_0}{Z_a + Z_0} \tag{21}$$

where $Z_0(=\rho_0 c_0)$ is the characteristic impedance of the branch or the medium. However, this reflection coefficient R is not equal to the reflection coefficient for

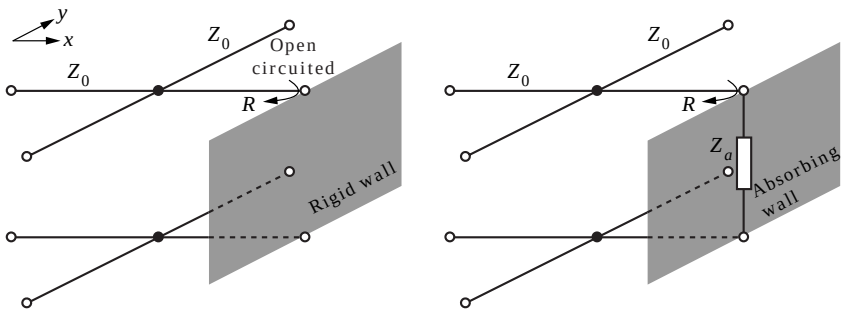

(a) Rigid wall (b) Absorbing wall

Figure 7. Branches contacting with typical boundaries.

the wave reflecting at the wall of the TLM network where the sound speed c_T is different from the one over a single arm or a branch. In this particular case for the wave perpendicularly incident into the wall, as shown in Figure 7(b) the reflection coefficient Γ is defined as

$$\Gamma = \frac{Z_a - Z_T}{Z_a + Z_T} \tag{22}$$

where $Z_T(= \rho_0 c_T)$ is the characteristic impedance for sound propagating in the network. Combining equations (21) and (22), one has the relation between R and Γ as

$$R = \frac{(1+\Gamma) - \sqrt{2}(1-\Gamma)}{(1+\Gamma) + \sqrt{2}(1-\Gamma)}. \tag{23}$$

To implement the reflection coefficient Γ into the TLM model, the following relation is applied:

$$_k P^n = R_k S^n. \tag{24}$$

In the special case of the non-reflective boundary in which Γ is set to 0, R is given as

$$R = \frac{1-\sqrt{2}}{1+\sqrt{2}}. \tag{25}$$

This non-reflective boundary condition is only exact for the case of perpendicular incidence. For waves striking the boundary at an arbitrarily incident angle, other treatments must be devised [12].

For the velocity drive, the pulse is excited on the branches of the elements. With the driving velocity u_0, the following pressure pulse train should be applied to the branch.

$$_kP^n = Z_T u_0. \tag{26}$$

2.4. MODELLING OF INHOMOGENEOUS AND LOSSY MEDIA

In the preceding discussions, we assumed that the medium was homogeneous and lossless. We here consider the more general cases of inhomogeneous and lossy media.

To vary the sound speed in the TLM element, a stub or an additional branch to the node is introduced as shown in Figure 8(a). The stub with length $\Delta l/2$ of characteristic admittance Y is open-circuited at another end. At the lower frequency range, the stub acts as a lumped shunt capacitance of $C\eta\Delta l/2$ where $\eta(=Y/Y_0)$ is normalized characteristic admittance and Y_0 is characteristic admittance of the main branches. Addition of the equivalent shunt capacitance to the node increases the equivalent medium compressibility. The total shunt capacitance at the node becomes

$$C' = 2C\Delta l(1 + \eta/4). \tag{27}$$

The sound speed c_T' in the two-dimensional TLM element with the open-circuited stub is thus given as

$$c_T' = \sqrt{\frac{2}{\eta + 4}}\, c_0. \tag{28}$$

The sound speed can be adjusted or decreased by varying the normalized characteristic admittance η of the additional stub in which the sound speed cannot exceed c_T because $\eta \geqslant 0$.

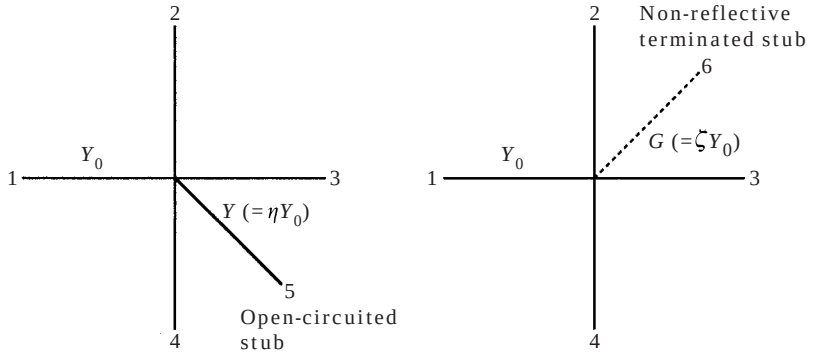

(a) TLM element with open stub (b) TLM element with sound absorbing stub

Figure 8. Two-dimensional TLM element with additional open stub branch and sound absorbing stub.

When a sound impulse of amplitude P is applied to the branch 1, the impulses scatter respectively in five directions. The scattering matrix with the open-circuited stub is given as

$$
{}_{k+1}\begin{bmatrix} S^1 \\ S^2 \\ S^3 \\ S^4 \\ S^5 \end{bmatrix} = \frac{2}{4+\eta} \begin{bmatrix} -1-\eta/2 & 1 & 1 & 1 & 1 \\ 1 & -1-\eta/2 & 1 & 1 & 1 \\ 1 & 1 & -1-\eta/2 & 1 & 1 \\ 1 & 1 & 1 & -1-\eta/2 & 1 \\ 1 & 1 & 1 & 1 & -2+\eta/2 \end{bmatrix} {}_{k}\begin{bmatrix} P^1 \\ P^2 \\ P^3 \\ P^4 \\ P^5 \end{bmatrix} \tag{29}
$$

where subscript 5 refers to the stub which is in fact not connected to any of the network. The impulse scattered at the node into the stub is then reflected at the open end and becomes the incident pulse into the same node, so that ${}_{k+1}P^5 = {}_{k+1}S^5$. The pressure at the node is given as

$$
{}_kP_{i,j} = \frac{2}{\eta+4} \sum_{n=1}^{4} {}_kP^n + \frac{2\eta}{\eta+4} {}_kP^5. \tag{30}
$$

To model the lossy medium, another 6th branch or a stub is introduced as illustrated in Figure 8(a), which provides a power dissipation. The stub with the conductance $G(=\zeta Y_0)$ is non-reflectively terminated at the other end. It corresponds to an additional shunt resistor to the node. The non-reflective termination at the stub end means that the stub is regarded as of infinite length

or terminated with the characteristic resistor (G) to match. The scattering matrix is thus given as

$$
{}_{k+1}\begin{bmatrix} S^1 \\ S^2 \\ S^3 \\ S^4 \\ S^6 \end{bmatrix} = \frac{2}{4+\zeta} \begin{bmatrix} -1-\zeta/2 & 1 & 1 & 1 & 0 \\ 1 & -1-\zeta/2 & 1 & 1 & 0 \\ 1 & 1 & -1-\zeta/2 & 1 & 0 \\ 1 & 1 & 1 & -1-\zeta/2 & 0 \\ 1 & 1 & 1 & 1 & 0 \end{bmatrix}
$$

$$
{}_{k}\begin{bmatrix} P^1 \\ P^2 \\ P^3 \\ P^4 \\ P^6 \end{bmatrix} \tag{31}
$$

where superscript 6 denotes the stub or 6th branch for the absorption. If both stubs are included together, the scattering matrices (29) and (31) are combined to give

$$
{}_{k+1}\begin{bmatrix} S^1 \\ S^2 \\ S^3 \\ S^4 \\ S^5 \end{bmatrix} = \frac{2}{4+\eta+\zeta} \begin{bmatrix} -1-(\eta+\zeta)/2 & 1 & 1 \\ 1 & -1-(\eta+\zeta)/2 & 1 \\ 1 & 1 & -1-(\eta+\zeta)/2 \\ 1 & 1 & 1 \\ 1 & 1 & 1 \end{bmatrix}
$$

$$
\begin{bmatrix} 1 & \eta \\ 1 & \eta \\ 1 & \eta \\ -1-(\eta+\zeta)/2 & \eta \\ 1 & (\eta-\zeta-4)/2 \end{bmatrix} {}_{k}\begin{bmatrix} P^1 \\ P^2 \\ P^3 \\ P^4 \\ P^5 \end{bmatrix} \tag{32}
$$

S^6 is missing in the equation as the pulse P^6 for the damping expression is not reflected back into the node. The pressure at the node is given as

$$
{}_kP_{i,j} = \frac{\eta+4}{\eta+\zeta+4}\left(\frac{2}{\eta+4}\sum_{n=1}^{4} {}_kP^n + \frac{2\eta}{\eta+4}\,{}_kP^5\right). \tag{33}
$$

Comparing equation (33) with equation (30), the damping ratio χ for an element is given as

$$\chi = \frac{\eta + 4}{\eta + \zeta + 4} \tag{34}$$

for which attenuation constant α is

$$\alpha = \frac{\sqrt{2}}{\Delta l} \ln \frac{\eta + 4}{\eta + \zeta + 4}. \tag{35}$$

Next the case of the discontinuous mass density of the media is considered. In order to simplify the question, the case in which the two media whose respective mass densities are ρ_1 and ρ_2 but whose sound speeds are the same is taken. This is illustrated in Figure 9(a). The reflection and the transmission take place at the interface between the two media due to the impedance discontinuity. The reflection and transmission coefficients at the interface are respectively given as

$$R_{11} = \frac{\rho_2 - \rho_1}{\rho_2 + \rho_1}, \quad T_{12} = \frac{2\rho_1}{\rho_2 + \rho_1}$$
$$T_{21} = \frac{2\rho_2}{\rho_1 + \rho_2}, \quad R_{22} = \frac{\rho_1 - \rho_2}{\rho_1 + \rho_2} \tag{36}$$

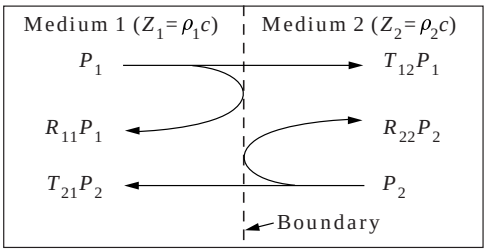

(a) Two-layered medium

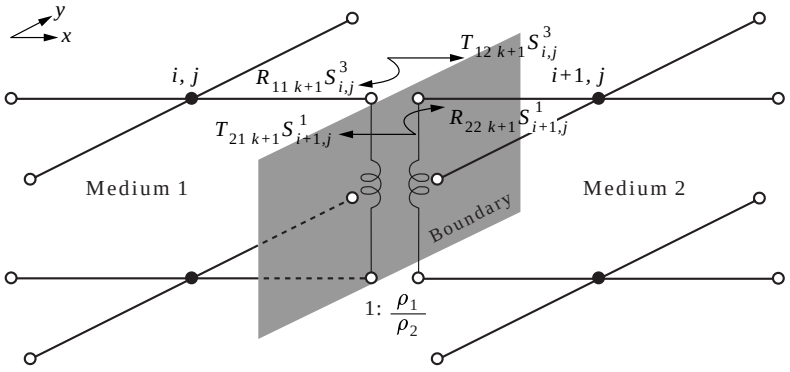

(b) TLM elements with different medium boundary

Figure 9. Reflection and transmission due to density discontinuity.

where the subscripts indicate each medium. To model such a situation, introduction is made for an ideal transformer of turn's ratio $1{:}\rho_1/\rho_2$ between the two media as shown in Figure 9(b). The reflection and transmission of the impulses are thus expressed as

$$\begin{bmatrix} {}_{k+1}P^3_{i,j} \\ {}_{k+1}P^1_{i+1,j} \end{bmatrix} = \begin{bmatrix} R_{11} & T_{12} \\ T_{21} & R_{22} \end{bmatrix} \begin{bmatrix} {}_{k+1}S^3_{i,j} \\ {}_{k+1}S^1_{i+1,j} \end{bmatrix}. \tag{37}$$

2.5. MODELLING OF AXISYMMETRIC FIELD

Since a scalar wave field is of interest, the three-dimensional axisymmetric field can simply be modelled as a two-dimensional field in which the medium density is the function of the radial distance as

$$\rho(r) = \frac{\rho_0}{2\pi r} \tag{38}$$

where r is the distance from the central axis. In this case, the characteristic impedance of each branch has a different value as shown in Figure 10 where r_j is the distance from the central axis to the node (i, j). The reflection coefficients from each branch are given as

$$\begin{gathered} R_1 = R_3 = -\tfrac{1}{2} \\ R_2 = -\frac{1}{2} + \frac{\Delta l}{4r_j}, \quad R_4 = -\frac{1}{2} - \frac{\Delta l}{4r_j}. \end{gathered} \tag{39}$$

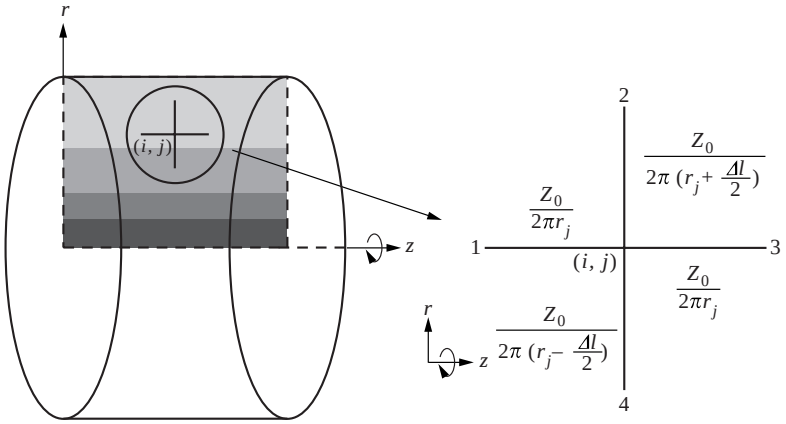

Figure 10. Characteristic impedance of each branch in an axisymmetric TLM element.

The scattering matrix is given as

$$
{}_{k+1}\begin{bmatrix} S^1 \\ S^2 \\ S^3 \\ S^4 \end{bmatrix} = \frac{1}{2}\begin{bmatrix} -1 & 1+\dfrac{\Delta l}{2r_j} & 1 & 1-\dfrac{\Delta l}{2r_j} \\ 1 & -1+\dfrac{\Delta l}{2r_j} & 1 & 1-\dfrac{\Delta l}{2r_j} \\ 1 & 1+\dfrac{\Delta l}{2r_j} & -1 & 1-\dfrac{\Delta l}{2r_j} \\ 1 & 1+\dfrac{\Delta l}{2r_j} & 1 & -1-\dfrac{\Delta l}{2r_j} \end{bmatrix} {}_{k}\begin{bmatrix} P^1 \\ P^2 \\ P^3 \\ P^4 \end{bmatrix}. \tag{40}
$$

2.6. ERROR ESTIMATION AND ERROR REDUCTION BY FILTERING

The discretization error for the TLM model is examined in this section. The relation between the incident pulses and the scattered pulses in the adjacent nodes surrounding a node can be written in terms of the pressure at the node. Substituting equations (1) and (3) into equation (4) and eliminating the pulses ${}_kP^1 \sim {}_kP^4$, we have the expression with respect to the pressure at a node and those surrounding it as follows

$$
{}_kP_{i-1,j} + {}_kP_{i+1,j} + {}_kP_{i,j-1} + {}_kP_{i,j+1} - 4_kP_{i,j} = 2({}_{k-1}P_{i,j} - 2_kP_{i,j} + {}_{k+1}P_{i,j}). \tag{41}
$$

This expression is the same as the finite difference–time domain (FD–TD) expression for a two-dimensional wave equation. Therefore TLM method is nothing but the FD–TD method's in numerical counterpart; while the TLM is a physical model, the FD–TD is a mathematical one. For error estimation, equation (41) is expanded into the Taylor series around ${}_kP_{i,j}$. Then the following differential equation results:

$$
\begin{aligned}
\frac{\partial^2{}_kP_{i,j}}{\partial x^2} + \frac{\partial^2{}_kP_{i,j}}{\partial y^2} = \frac{1}{c_T^2}\frac{\partial^2{}_kP_{i,j}}{\partial t^2} \\
- \frac{2}{\Delta l^2}\left\{\frac{\Delta l^4}{4!}\left(\frac{\partial^4{}_kP_{i,j}}{\partial x^4} + \frac{\partial^4{}_kP_{i,j}}{\partial y^4}\right) + \frac{\Delta l^6}{6!}\left(\frac{\partial^6{}_kP_{i,j}}{\partial x^6} + \frac{\partial^6{}_kP_{i,j}}{\partial y^6}\right) + \cdots\right\} \\
+ \frac{4}{\Delta l^2}\left\{\frac{\Delta t^4}{4!}\frac{\partial^4{}_kP_{i,j}}{\partial t^4} + \frac{\Delta t^6}{6!}\frac{\partial^6{}_kP_{i,j}}{\partial t^6} + \cdots\right\}.
\end{aligned} \tag{42}
$$

This differential equation expresses the wave over the two-dimensional TLM network in which the higher order terms are due to the discretization. The higher order terms lead to the fluctuation error in the discretized simulation. The error becomes larger where the sound pressure rapidly changes with time and space. As in the other numerical methods, the TLM method also requires the fine mesh for an accurate solution.

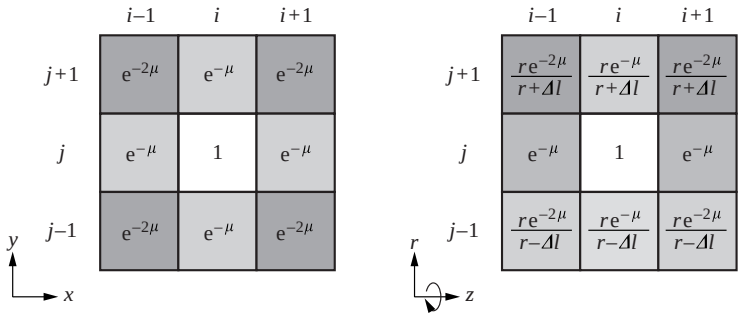

(a) Two-dimensional field (b) Axisymmetric field

Figure 11. Weighting matrix for Gaussian spatial filtering.

In the axisymmetric case, the following differential equation results:

$$\frac{\partial^2{}_k P_{i,j}}{\partial r^2} + \frac{1}{r}\frac{\partial_k P_{i,j}}{\partial r} + \frac{\partial^2{}_k P_{i,j}}{\partial z^2} = \frac{1}{c_T^2}\frac{\partial^2{}_k P_{i,j}}{\partial t^2}$$

$$- \frac{2}{\Delta l^2}\left\{\frac{\Delta l^4}{4!}\left(\frac{\partial^4{}_k P_{i,j}}{\partial r^4} + \frac{\partial^4{}_k P_{i,j}}{\partial z^4}\right) + \frac{\Delta l^6}{6!}\left(\frac{\partial^6{}_k P_{i,j}}{\partial r^6} + \frac{\partial^6{}_k P_{i,j}}{\partial z^6}\right) + \cdots\right\}$$

$$+ \frac{4}{\Delta l^2}\left\{\frac{\Delta t^4}{4!}\frac{\partial^4{}_k P_{i,j}}{\partial t^4} + \frac{\Delta t^6}{6!}\frac{\partial^6{}_k P_{i,j}}{\partial t^6} + \cdots\right\}$$

$$- \frac{1}{r\Delta l}\left\{\frac{\Delta l^3}{3!}\frac{\partial^3{}_k P_{i,j}}{\partial r^3} + \frac{\Delta l^5}{5!}\frac{\partial^5{}_k P_{i,j}}{\partial r^5} + \cdots\right\}. \tag{43}$$

It has the same order of the higher terms as in the two-dimensional case, in which additional terms with $1/r$ are present. Due to these terms, the error increases as the node is placed closer to the central axis.

To reduce fluctuation errors due to the higher order terms, a two-dimensional Gaussian filter is devised into the TLM as is used for graphical processing. The pressure $P_{i,j}$ at the node is obtained by averaging the pressures at the adjacent nodes which are weighted by the coefficient matrix as shown in Figure 11(a). The pressure $\overline{P}_{i,j}$ is now evaluated as

$$\overline{P}_{i,j} = \{P_{i,j} + \mathrm{e}^{-\mu}(P_{i-1,j} + P_{i+1,j} + P_{i,j-1} + P_{i,j+1})$$

$$+ \mathrm{e}^{-2\mu}(P_{i-1,j-1} + P_{i+1,j-1} + P_{i-1,j+1} + P_{i+1,j+1})\}/(1 + 4\mathrm{e}^{-\mu} + 4\mathrm{e}^{-2\mu}) \tag{44}$$

where μ is a parameter to be controlled. This is a spatial or two-dimensional low-pass filter. To implement the algorithm, the first term of the right-hand side of equation (1) is replaced by equation (44). For the axisymmetric case, the weighting matrix is also shown in Figure 11(b).

2.7. MODELLING OF A NON-LINEAR MEDIUM

We here include the non-linearity in a medium. The non-linear effect is essentially caused by the dependence of the sound speed on the local sound pressure, which is expressed as follows [13–15]:

$$c_n(p) = \left(1 + \frac{vp}{\rho_0 c_0^2}\right) c_0 \tag{45}$$

where p is local sound pressure, v is non-linear parameter of the medium, ρ_0 is the density of the medium and c_0 is the sound speed for small amplitude wave. The sound pressure waveform distorts as it propagates due to this pressure dependence of the speed.

To implement the non-linear effect into the TLM model, the sound speed is made a function of the sound pressure at the node by adjusting the admittance of the additional stub as previously discussed in Figure 8. When the normalized admittance changes by as small as $\Delta\eta$ from η_0 due to the non-linearity of the medium, the sound speed is given as

$$c_n = \sqrt{\frac{2}{(\eta_0 + \Delta\eta) + 4}}\, c_0 \doteqdot \left(1 - \frac{1}{2}\frac{\Delta\eta}{\eta_0 + 4}\right) c_T' \tag{46}$$

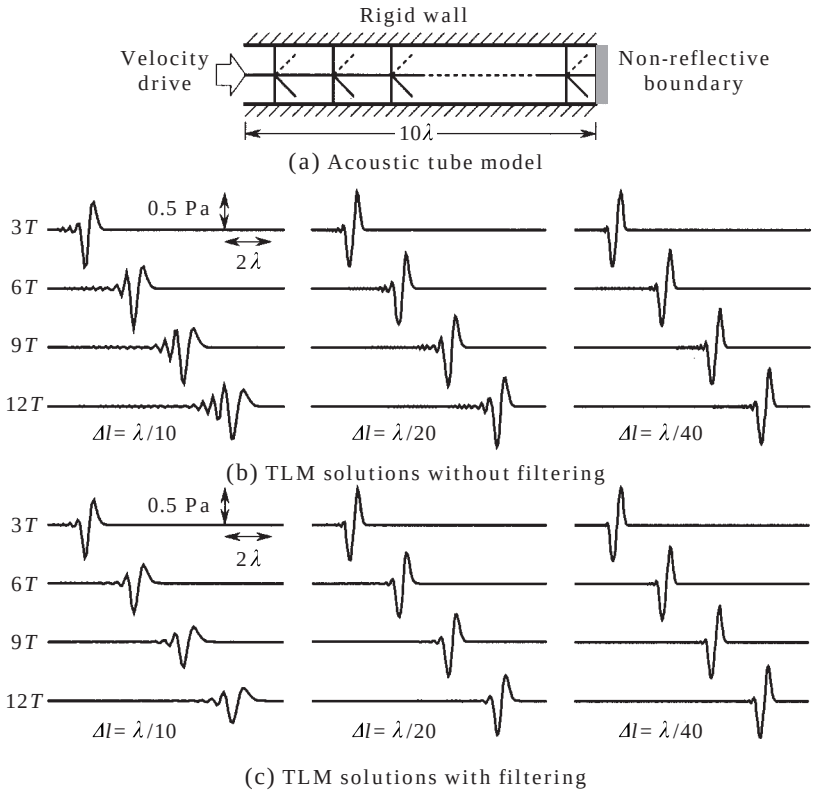

Figure 12. Acoustic tube model and TLM solutions for a single-shot sine wave ($\eta = 0, \zeta = 0, \mu = 0$) and solutions with the filtering capability ($\mu = 5$).

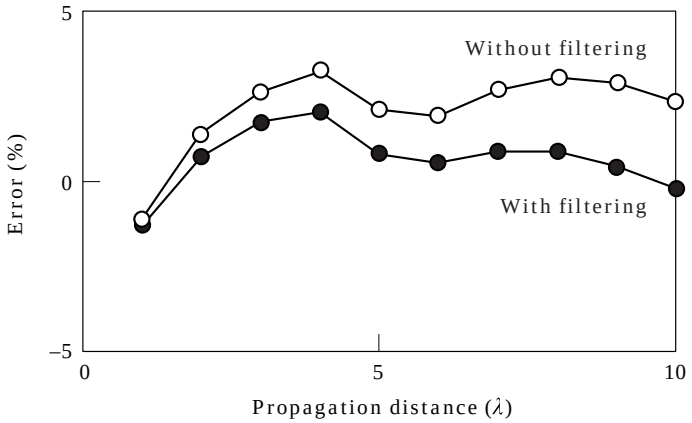

Figure 13. Relation between the propagation distance and the evaluation error with respect to peak-to-peak pressure evaluation ($\Delta l = \lambda/40$).

where c_T' is given in equation (28) which is linear. Comparing the ratio of increase of the sound speed in equations (45) and (46), one obtains the expression for $\Delta\eta$

$$\Delta\eta = -\frac{(2\eta_0 + 8)v}{\rho_0 c_0^2} p. \tag{47}$$

The non-linear effect can thus easily be introduced into the TLM by varying the local sound speed. In equation (47), the condition $\eta_0 + \Delta\eta > 0$ is required for stable calculation.

3. NUMERICAL EXAMPLES

3.1. QUASI-ONE-DIMENSIONAL FIELD

To check the validity of the TLM modelling as proposed, the simple problem of a plane wave propagation in an acoustic tube is first examined. The tube is

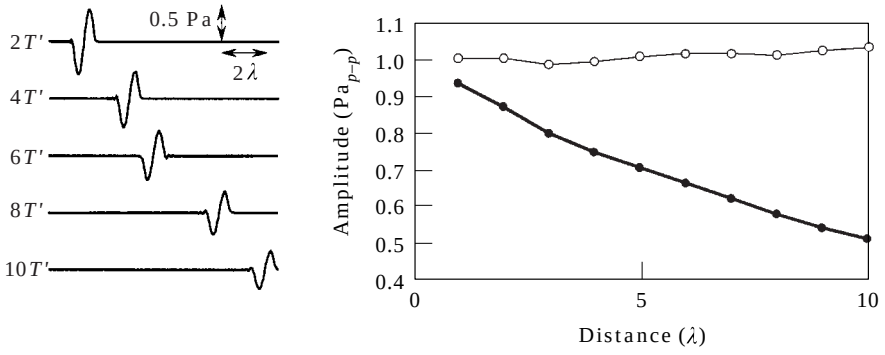

(a) Wave travelling (ζ=5×10^{-3}) (b) Propagation characteristics

Figure 14. A single-shot sine wave traveling through the lossy medium and its propagation characteristics ($\zeta = 5 \times 10^{-3}$, $\Delta l = \lambda/40$). ○, without damping; ●, with damping ($\zeta = 5 \times 10^{-3}$).

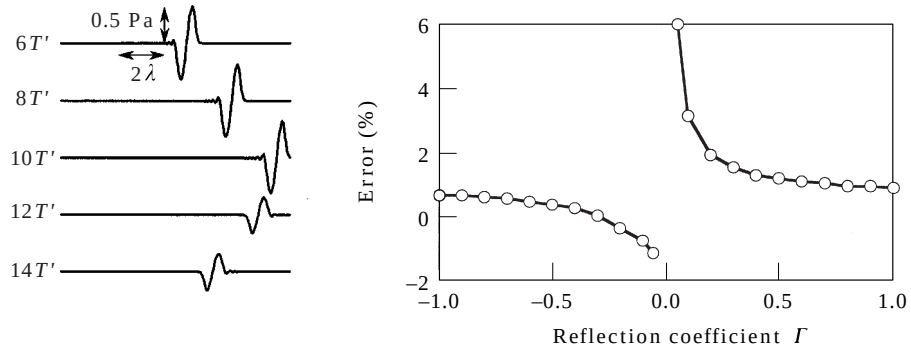

(a) Wave travelling ($R = -0.5$) (b) Relation between the reflection coefficient and the calculation error

Figure 15. Wave reflected from the end wall and the relation between the reflection coefficient and the error ($\Delta l = \lambda/40$).

modelled as a series of TLM elements as shown in Figure 12(a). In the model, one end of the tube is terminated by the non-reflective boundary while another end is driven by the velocity source of a train of pulses of single-shot sine envelope with wavelength λ and the side walls are considered to be rigid. The element length Δl is chosen to be from $\lambda/10$ to $\lambda/40$ in order to check the accuracy.

Figure 12(b) shows the pressure waveforms as the sine wave with the amplitude of 0·5 Pa propagates until the time $12T$, where T is the period of the sine wave. It is shown that the wave propagates at the speed of $c_0/\sqrt{2}$ as expected in equation (11). The fluctuation errors become pronounced as the wave propagates. This is due to the presence of the higher order error terms resulting from the discretization as expected in equation (42). The fluctuation decreases as the element length becomes shorter. As with other numerical methods, the TLM method also requires the fine mesh for an accurate solution. To reduce fluctuation errors, the two-dimensional Gaussian filter as given by equation (44) is devised. The solutions with the filtering are shown for $\mu = 5$ in Figure 12(c). In this simulation the filtering processing is provided every quarter of the period or T. The filtering reduces the fluctuation at the expense of the slightly damped amplitude. Figure 13 shows a relation between the propagation distance and the error for the peak-to-peak amplitude of the sine wave. The error increases as the wave propagates, but the accuracy is practically satisfactory as it is within a few percent at each propagation distance of the wavelength. The element size should be chosen smaller than one-fortieth of the wavelength to achieve a practically admissible accuracy.

Next demonstration is made for the capability of the modelling for the wave propagating through the lossy media. The damping parameter ζ is chosen to be 5×10^{-3} which is equivalent to the attenuation constant α of $7{\cdot}07 \times 10^{-2}$ (neper/λ). The propagation of a sine wave is shown in Figure 14(a). In the figure, $T' = T/\sqrt{2}$ is the period in free space. The amplitude damps as the wave propagates. Figure 14(b) shows the propagation characteristics. Fine and bold lines indicate the cases without and with damping respectively. The amplitude

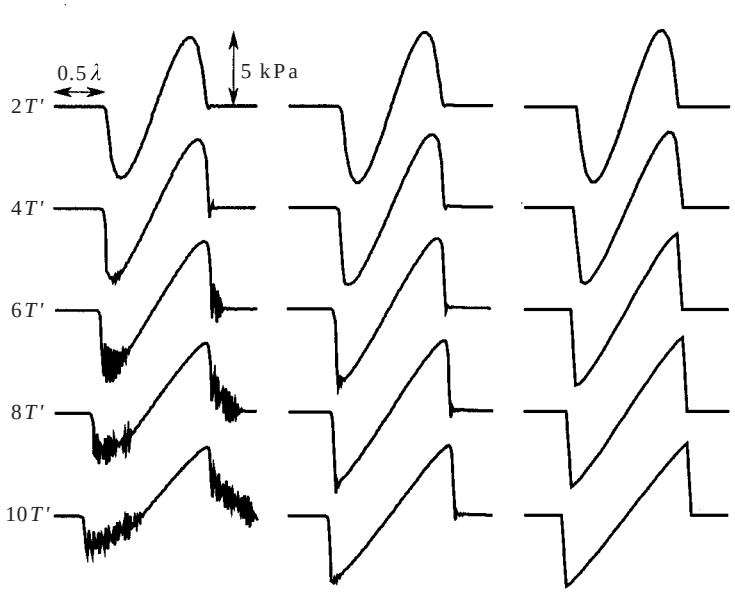

Figure 16. Non-linear wave propagation for a single-shot sine wave ($P = 5$ kPa, $\Delta l = \lambda/200$).

damps exponentially with the propagation. The attenuation constant α is estimated from the figure to be $7{\cdot}09 \times 10^{-2}$ (neper/λ) which is in good agreement with the original value.

To check the boundary condition, the reflection from the absorbing non-reflective wall is examined. The model is almost the same as in Figure 12(a) but the end of the tube is terminated by a certain impedance. The wave

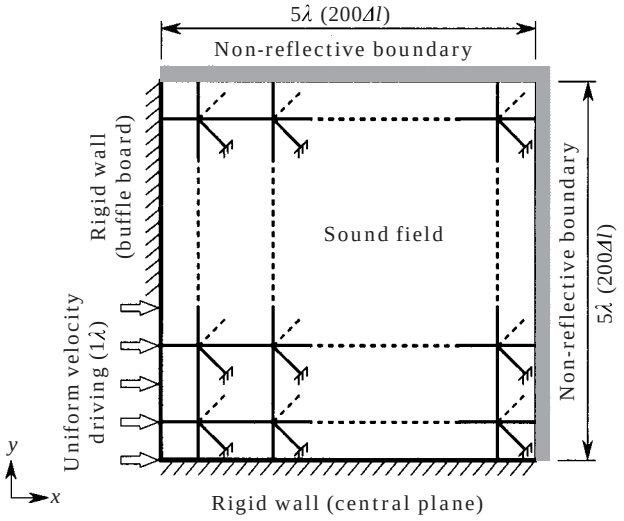

Figure 17. Two-dimensional field and TLM network.

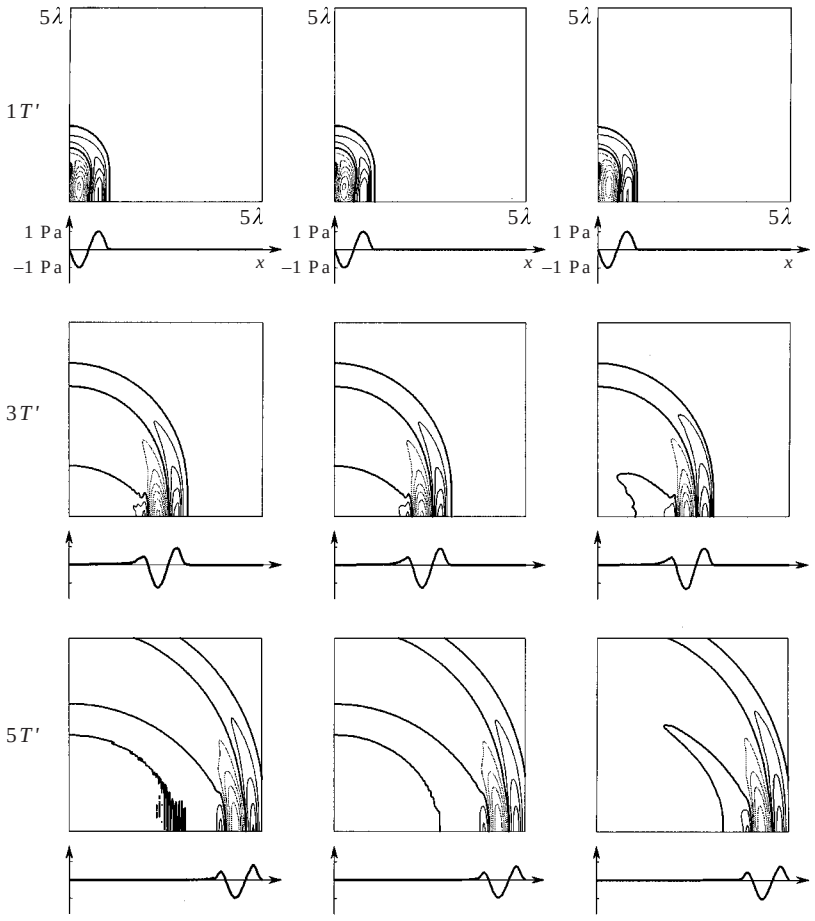

Figure 18. Linear wave propagation for a single-shot sine wave in the two-dimensional field ($P = 1$ Pa, $\Delta l = \lambda/40$).

propagation and the reflection from the wall are shown in Figure 15(a) in the case for $\Gamma = -0{\cdot}5$. Figure 15(b) shows the relation between the reflection coefficient Γ and the error of the TLM solution. Though the error increases as Γ closes to 0, the practically admissible accuracy of a few percent is achieved.

The examination is then extended to the non-linear medium for which air is assumed (sound speed $c_o = 340$ m/s, density $\rho_0 = 1{\cdot}2$ kg/m^3 and non-linearity parameter $\nu = 1{\cdot}2$). The model shown in Figure 12(a) is again used. Other parameters are the same as in the linear case except that Δl is chosen to be as small as $\lambda/200$. The non-linear propagation is simulated for a single-shot sine wave with the amplitude of 5 kPa. Figure 16 shows the pressure waveform transformation up to the time $10T'$. Figure 16(a) and (b) are the TLM solutions without and with Gaussian filtering and Figure 16(c) is the analytical solutions [16, 17]. The filtering operation is devised for each time step. The solutions are not stable without filtering as shown in Figure 16(a). Its introduction helps to reduce the fluctuations

as shown in Figure 16(b). The filter acts as an artificial viscosity which is sometimes introduced to suppress the instability in the numerical calculation of fluid dynamics. The waveforms distort as they propagate and the shock finally develops. The TLM solutions with filtering agree well with the analytical solutions. Non-linear sound propagation can thus be simulated with reasonable accuracy by introducing the Gaussian spatial filtering.

3.2. TWO-DIMENSIONAL FIELD

We proceed to the wave propagation in the two-dimensional field. The two-dimensional sound field as shown in Figure 17 is taken. A plane piston source with the width of the half wavelength $\lambda/2$ is uniformly driven by the single-shot sine wave. The square area of side length of 5λ is taken. The medium is assumed to be air. The buffle board outside the piston is assumed to be rigid and the other boundaries are terminated by non-reflective boundary condition. Only a

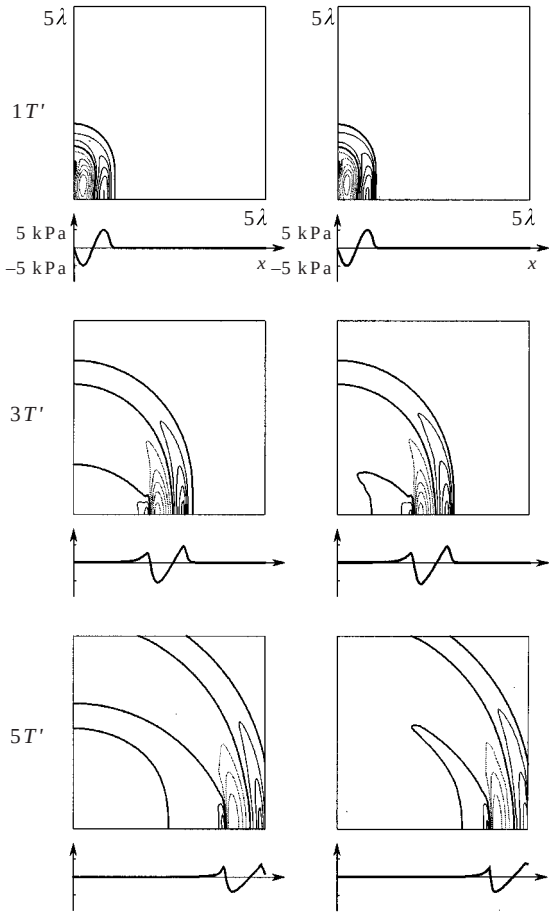

Figure 19. Non-linear wave propagation for a single-shot sine wave in the two-dimensional field ($P = 5$ kPa, $\Delta l = \lambda/40$).

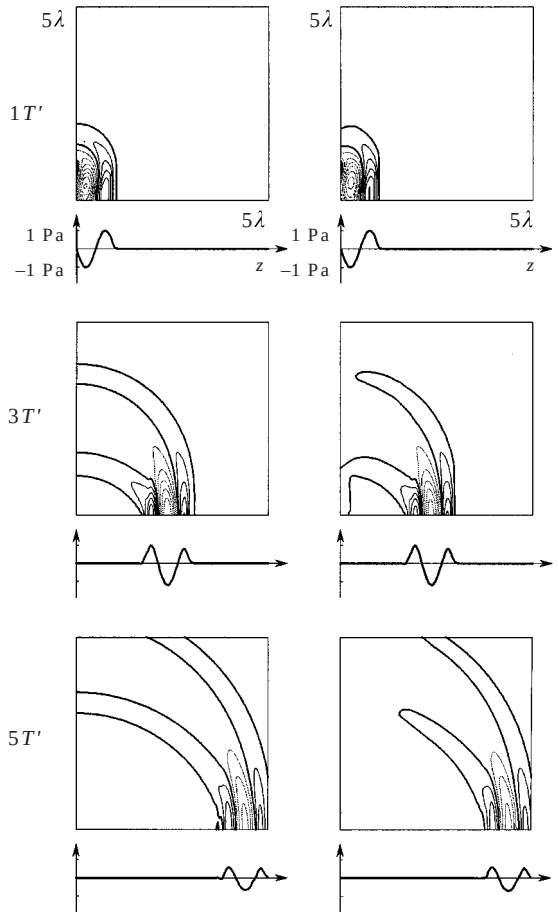

Figure 20. Linear wave propagation for a single-shot sine wave in the axisymmetric field ($P = 1$ Pa, $\Delta l = \lambda/40$).

half-region is taken because the central plane of symmetry is taken to be rigid. The element length Δl is chosen to be $\lambda/40$.

The linear wave propagation of the amplitude of 1 Pa is illustrated until the time $5T'$ in Figure 18. Figure 18(a) and (b) show the TLM solutions without and with Gaussian filtering, and Figure 18(c) finite element solutions with 200×200 first order triangular elements. For the FEM, the time step Δt is chosen to be $T/400$. Though the fluctuation errors also appear in the two-dimensional solutions as the wave propagates, they can be reduced with the use of Gaussian filtering. The TLM solutions show good agreement with the finite element solutions.

For the non-linear case, the amplitude is increased to 5 kPa. Other parameters are the same as in the linear case. The non-linear wave propagation is illustrated until the time $5T'$ in Figure 19. Figure 19(a) shows the TLM solutions with filtering and Figure 19(b) shows the finite element solutions with second order triangular elements. The waveform is again distorted as it propagates until the weak shock develops. The TLM solutions again agree well with the finite element solutions.

3.3. AXISYMMETRIC THREE-DIMENSIONAL FIELD

The wave propagation in the axisymmetric three-dimensional field is finally considered. The cross-sectional area to be examined is the same as the two-dimensional case except that the x and y axes are replaced by the z and r axes in the axisymmetric case in which integration is carried out around the θ-circumferential direction. A circular piston source with a radius of 1λ is uniformly driven by the single-shot sine wave. Other conditions are the same as in the two-dimensional case.

The linear wave propagation with the amplitude of 1 Pa is illustrated until time $5T'$ in Figure 20. Figure 20(a) shows the TLM solutions with Gaussian filtering and Figure 20(b) shows the finite element solutions with 200×200 first order triangular ring elements. For the axisymmetric case, the TLM solutions again show good agreement with the finite element solutions.

4. CONCLUDING REMARKS

A discrete Huygens' model is proposed which is a synonym of the transmission-line matrix method, applied to the simulation of sound wave propagation. The two-dimensional and axisymmetric TLM elements are obtained for the sound field. Analogous and digital equivalent circuit expressions are developed for the two-dimensional TLM elements. Their transfer characteristics are examined theoretically. The discretization error is then considered and the reduction technique is proposed using Gaussian filtering. It is found that the Gaussian spatial filtering is necessary for non-linear wave propagation simulation. The TLM solutions agree well with the analytical solutions. Some numerical examples are demonstrated for two-dimensional and axisymmetric sound radiation. Verifications are also made compared with the finite element solutions. Wave propagations in the two-dimensional and axisymmetric field problems are simulated on a computer and its validity and accuracy are examined for a plane wave in an acoustic tube. The simulation shows that element size should be chosen smaller than one-fortieth of the wavelength for reasonable accuracy and Gaussian filtering is effective in reducing discretization errors. The modelling is extended to the cases when the medium is non-linear. It is confirmed that the TLM approach is useful in the time-domain analysis of both linear and non-linear sound propagation.

REFERENCES

1. P. B. JOHNS and R. L. BEURLE 1971 *Proc. Inst. Elec. Eng.* **118**, 1203–1208. Numerical solution of 2-dimensional scattering problems using a transmission-line matrix.
2. P. B. JOHNS 1974 *IEEE Trans. Microwave Theory and Techniques* **MTT-22**, 209–215. The solution of inhomogeneous waveguide problems using a transmission-line matrix.
3. W. J. R. HOEFER 1985 *IEEE Trans. Microwave Theory and Techniques* **MTT-33**, 882–893. The transmission-line matrix method—theory and applications.
4. W. J. R. HOEFER 1991 *Proceedings of IEEE* **79**, 1459–1471. Huygens and the computer—a powerful alliance in numerical electromagnetics.

5. M. N. O. Sadiku and L. C. Agba 1990 *IEEE Trans. Circuits and Systems* **CAS-37**, 991–999. A simple introduction to the transmission-line modeling.
6. Directed by W. J. R. Hoefer and R. Vahldieck 1977 *Workshop Digest of the First International Workshop on Transmission Line Matrix (TLM) Modeling—Theory and Applications*, Victoria, Canada.
7. Y. Yoshii, T. Yamabuchi and Y. Kagawa 1976 *Proc. Spring Meet. Acoust. Soc. Jpn.* **3-5-10**, 421–422. An application of transmission-line matrix method to acoustical field problems (in Japanese).
8. Y. Yoshii (supervisor: Y. Kagawa) 1977 *M.Sc. thesis*, *Toyama University*, *Japan*. Acoustic field analysis by TLM method (in Japanese).
9. A. H. M. Saleh and P. Blanchfield 1990 *Int. J. Numerical Modeling*: *Electronic Networks*, *Devices and Fields* **3**, 39–56. Analysis of acoustic radiation patterns of array transducers using the TLM method.
10. Y. Kagawa and T. Yamabuchi 1978 *J. Acoust. Soc. Am.* **64**, 1196–1200. Finite-element equivalent circuits for acoustic field.
11. Y. Kagawa 1977 *Ohm-sha*, *Tokyo*. Finite element methods for electrical engineers (in Japanese).
12. J. A. Morente, J. A. Portí and M. Khalladi 1992 *IEEE Trans. on Microwave Theory and Techniques* **MTT-40**, 2095–2099. Absorbing boundary conditions for the TLM method.
13. D. T. Blackstock 1972 *American Institute of Physics Handbook*, (D. Gray, editor), Chap. 3n, Nonlinear Acoustics (Theoretical). New York: McGraw–Hill.
14. T. Tsuchiya, Y. Watanabe and Y. Urabe 1988 *J. Acoust. Soc. Jpn.* **44**, 669–672. Theoretical approach for the virtual source on the view of the distortion of the finite–amplitude wave (in Japanese).
15. Y. Kagawa, T. Tsuchiya, T. Yamabuchi, H. Kawabe and T. Fujii 1992 *J. Sound and Vib.* **154** (1), 125–145. Finite element simulation of non-linear sound wave propagation.
16. H. Mitome 1989 *J. Acoust. Soc. Am.* **86**, 2334–2338. An exact solution for the finite–amplitude plane sound waves on a dissipative fluid.
17. T. Tsuchiya and Y. Kagawa 1992 *J. Acoust. Soc. Jpn.* (*E*) **13** (4), 223–230. A simulation study on nonlinear sound propagation by finite element approach.